Figures and figure supplements

BK channel properties correlate with neurobehavioral severity in three *KCNMA1*-linked channelopathy mouse models

Su Mi Park *et al*

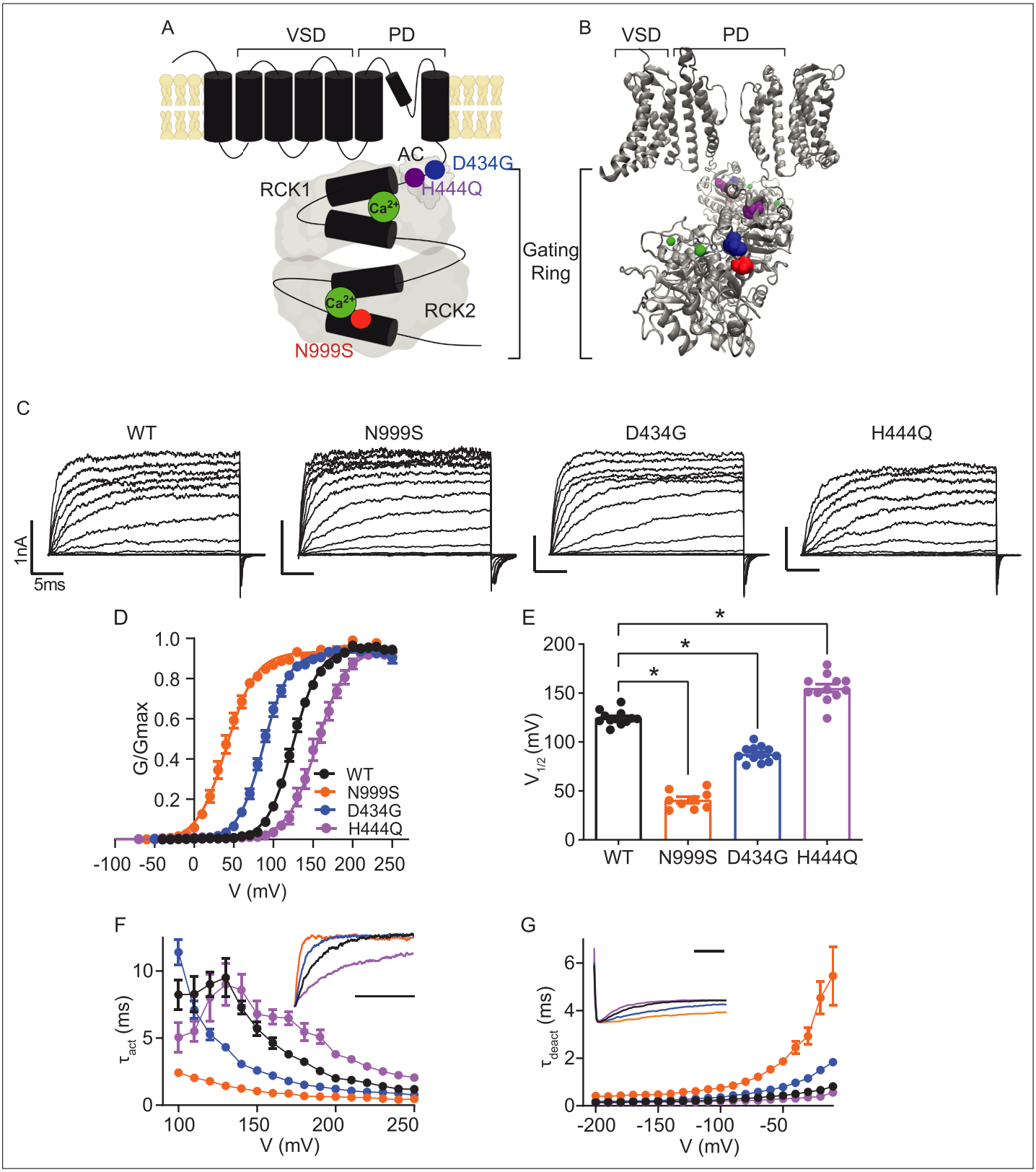

Figure 1. Location and consequence of *KCNMA1* variants in the BK K^+ channel. (**A**) *KCNMA1* forms the homotetrameric BK channel. Each α subunit is comprised of seven transmembrane domains (S0–S6) and an intracellular gating ring with hydrophobic segments (S7–S10, black). Pore (+) opening and closing is regulated by voltage-sensitive residues in S2–S4 (VSD), the AC domain (βA to αC), and two Regulators of Conductance of Potassium (RCK) domains in the gating ring (gray), each containing a Ca^{2+} binding site (green) (***Yang et al., 2015***; ***Giraldez and Rothberg, 2017***). (**B**) BK channel

Figure 1 continued on next page

Figure 1 continued

structure showing two opposing subunits with Ca^{2+} bound in the gating ring (PDB 6V38). H444Q (purple) and D434G (blue) are located within the βB-αB and αA and βB of the AC domain, respectively, a region within RCK1 affecting Ca^{2+}-dependent gating (***Du et al., 2005***; ***Tao and MacKinnon, 2019***). N999S (red) is located at the helix bend in the middle of the S10 domain within RCK2 (***Tao and MacKinnon, 2019***). (**C**) Representative inside-out patch-clamp recordings from BK^{WT}, BK^{N999S}, BK^{D434G}, BK^{H444Q} channels expressed in HEK293 cells. Macroscopic BK currents were recorded in symmetrical K^+ and 1 μM intracellular Ca^{2+} by holding patches at −100 mV, stepping from −100 to 250 mV for 30 ms, followed by a tail step −100 mV for 15 ms. Scale bars: 1 nA, 5 ms. (**D**) Normalized conductance-voltage (G-V) relationships fit with Boltzmann functions (solid lines). There was no change in the slope factor (**z**) for any of the variants (p=0.06, one-way ANOVA). BK^{WT} (n=12), BK^{N999S} (n=9), BK^{D434G} (n=12), and BK^{H444Q} (n=12). (**E**) Voltage of half-maximal activation ($V_{1/2}$) obtained from Boltzmann fits for individual patches. *p<0.0001. One-way ANOVA with Dunnett's post hoc. (**F**) Activation time constants (τ_{act}). BK^{N999S} and BK^{D434G} channels had decreased τ_{act} compared to BK^{WT}, either across all voltage steps (mixed effects model for repeated measures with Bonferroni post hoc, p<0.01) or above 120 mV (p<0.05), respectively. At lower voltages, BK^{D434G} channels were more steeply voltage dependent, but did not exceed the fast activation time constants of BK^{N999S} channels. BK^{H444Q} channels had increased τ_{act} compared to BK^{WT} between 160 and 250 mV (p<0.05). *Inset*: Representative current traces from 170 mV step, scaled to the maximal current to illustrate activation timecourse (x-axis scale bar: 10 ms). τ_{act} for BK^{WT} currents was 3.8±0.3 ms, while BK^{N999S} and BK^{D434} currents activated faster (0.9±9.1 and 1.8±0.1 ms, respectively) and BK^{H444Q} activated slower (6.5±0.5 ms). (**G**) Deactivation time constants (τ_{deact}). BK^{N999S} and BK^{D434G} channels had increased τ_{deact} compared to BK^{WT}, across all voltage steps (mixed effects model for repeated measures with Bonferroni post hoc, p<0.01), with the exception of −160 (p>0.05), respectively. BK^{H444Q} channels had decreased τ_{deact} compared to BK^{WT} between −190 mV and between −140 and −20 mV (p<0.05). *Inset*: Representative current traces from −20 mV step, scaled to the maximal current to illustrate deactivation timecourse (x-axis scale bar: 10 ms). τ_{deact} for BK^{WT} currents was 0.7±0.01 ms, while BK^{N999S} and BK^{D434} currents deactivated slower (4.5±0.7 and 1.5±0.1 ms, respectively) and BK^{H444Q} deactivated more quickly (0.4±0.01 ms). Data are presented as mean ± SEM. Additional data on the effects of stimulants on BK^{WT} and BK^{N999S} channels appears in ***Figure 1—figure supplement 1***.

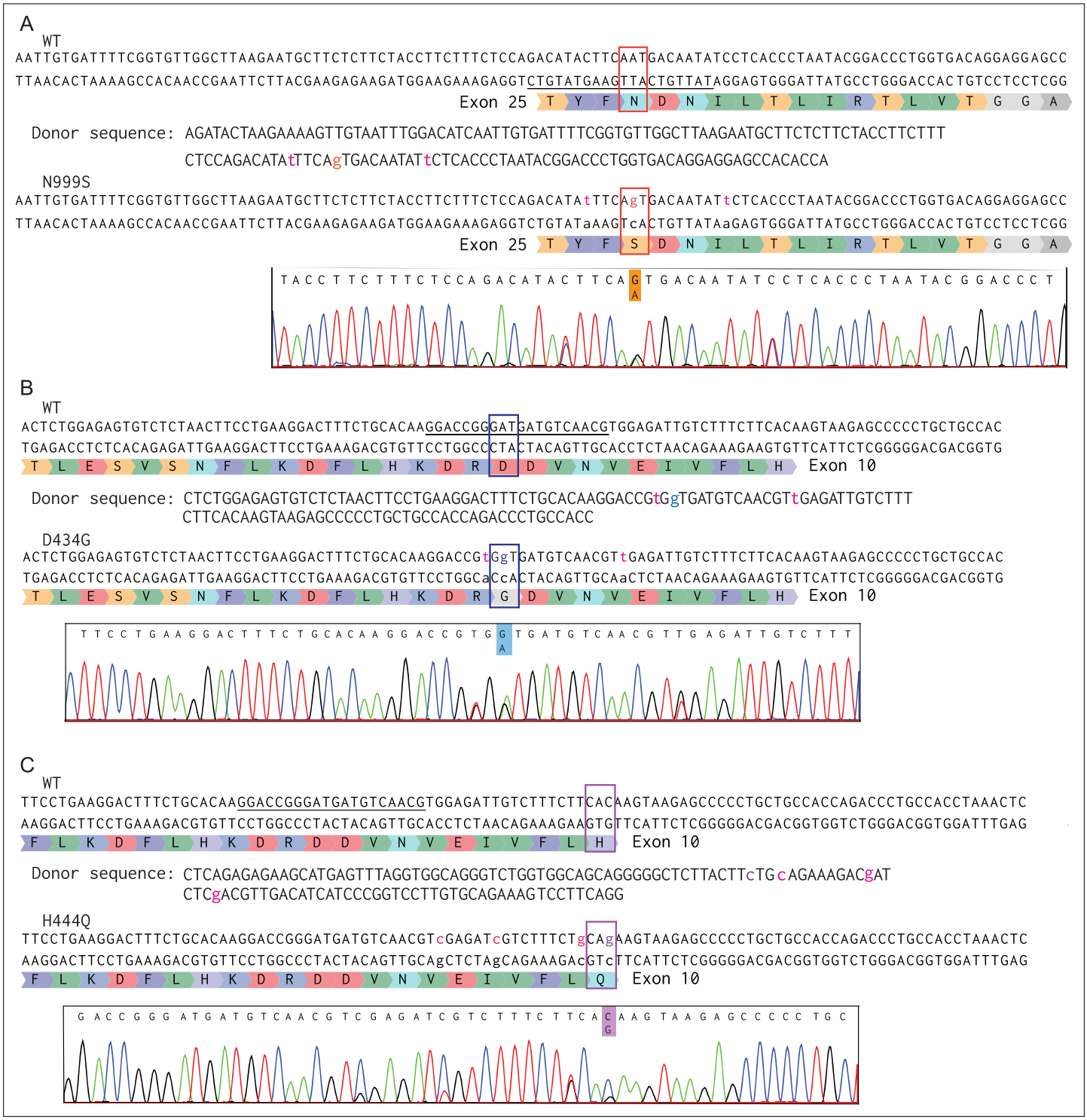

Figure 1—figure supplement 1. Sequences for CRISPR/Cas9 editing of the mouse *Kcnma1* gene. (**A**) *Kcnma1*$^{N999S/WT}$ mice were generated by introducing a non-synonymous mutation within the codon AAT→ AgT (red boxes) in exon 25. WT sequence is C57BL/6J. Underlined nucleotides are the gRNA sequence. Lowercase letters denote mutations. Chromatogram from an N1 heterozygous mouse. (**B**) *Kcnma1*$^{D434G/WT}$ mice were generated by mutation within the codon GAT→ GgT in exon 10. Chromatogram from a founder mouse. (**C**) *Kcnma1*$^{H444Q/WT}$ mice were generated by mutation within the codon CAC → CAg in exon 10 (same guide RNA as D434G). Chromatogram from a founder mouse.

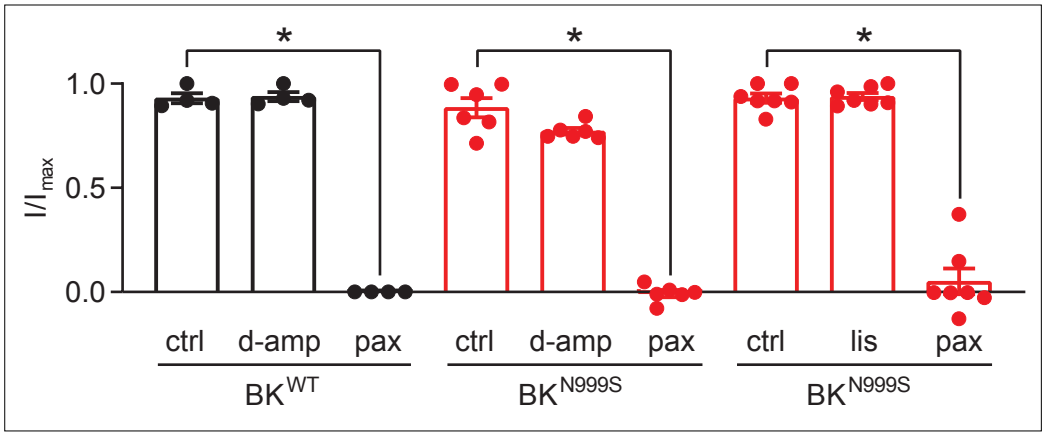

Figure 1—figure supplement 2. Effects of lisdexamfetamine (lis) and dextroamphetamine (d-amp) on BK^{WT} and BK^{N999S} channels expressed in HEK293 cells. D-amp and lis, a prodrug of D-amphetamine and L-lysine, have been reported to treat paroxysmal non-kinesigenic dyskinesia (PNKD) episodes in six children harboring N999S variants, as well as one child harboring another gain-of-function (GOF) variant (***Miller et al., 2021***; ***Zhang et al., 2020***). To test if either drug has a direct effect on BK currents in heterologous cells, as has been suggested for methamphetamine (***Lin et al., 2016***; ***Fu et al., 2021***; ***Tatro et al., 2013***; ***Wang et al., 2013***), d-amp and lis were applied to patches from HEK293 cells expressing BK^{WT} or BK^{N999S}. Macroscopic BK currents were evaluated after perfusion of each drug and compared to pre-drug control current levels. Normalized data presented as the proportion of the maximal current (I/I_{max}) for each patch, before (control) and after drug application. Neither 155 ng/ml lis (BK^{N999S}: n=7, p=0.98; one-way ANOVA) nor 155 ng/ml d-amp (BK^{WT}: n=4, p=0.99; one-way ANOVA and BK^{N999S}: n=6, p=0.15; one-way ANOVA) produced a decrease in BK current levels. However, the BK channel inhibitor paxilline (pax, 100 nM), applied as a control, fully abrogated BK^{WT} or BK^{N999S} currents at the end of each experiment ($p<0.001$; one-way ANOVA for all). Data are presented as mean ± SEM.

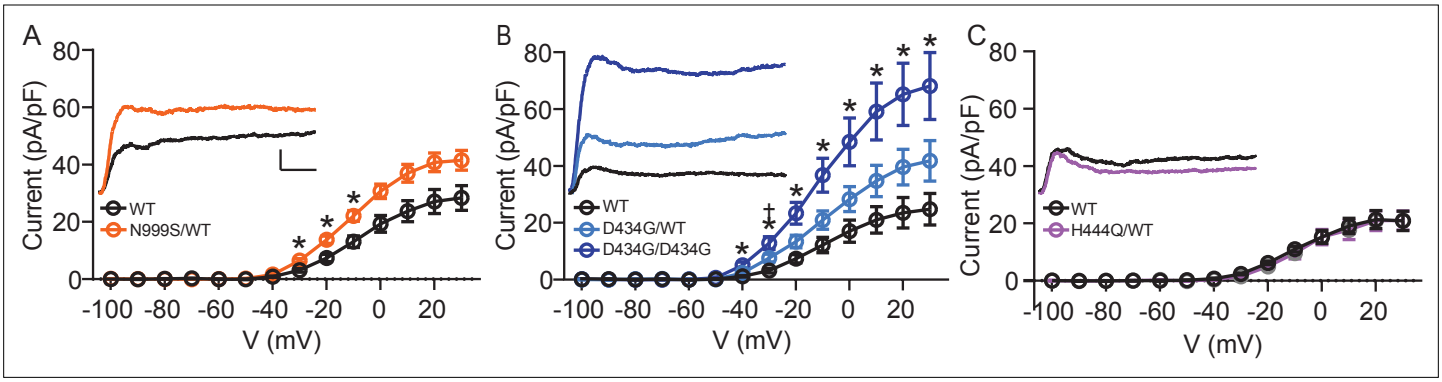

Figure 2. Increased BK current in *Kcnma1*$^{N999S/WT}$ and *Kcnma1*$^{D434G/D434G}$ granule neurons. Whole-cell macroscopic BK currents were recorded in 1 µM tetrodotoxin (TTX) and 2 mM 4-aminopyridine (4-AP), isolated with 10 µM paxilline, and normalized to cell capacitance. Activating voltage steps were applied from V_h of −90 mV, stepping from −100 to +30 mV for 150 ms, and back to −90 mV for 130 ms. (A–C) Peak BK current density versus voltage relationships. Data are presented as mean ± SEM. * and †, p<0.05, two-way repeated measures ANOVA with Bonferroni post hoc. *Insets:* Representative BK current traces at 30 mV. Scale bars: 500 pA, 5 ms. (**A**) BK current density was larger in *Kcnma1*$^{N999S/WT}$ neurons (n=16 neurons, 5 mice) compared to *Kcnma1*$^{WT/WT}$ (n=14 neurons, 4 mice) at −30 mV (p=0.0114), −20 (p=0.0210), −10 (p=0.0426) voltage steps (indicated with *). (**B**) BK current density was larger in *Kcnma1* $^{D434G/D434G}$ neurons (n=12 neurons, 3 mice) compared to *Kcnma1*$^{WT/WT}$ (n=10 neurons, 4 mice) at density at −40 mV (p=0.0112), −30 (p=0.0026), −20 (p=0.0031), −10 (p=0.0038), 0 (p=0.0078), 10 (p=0.0068), 20 (p=0.0071), 30 (p=0.0088) voltage steps (*). *Kcnma1*$^{D434G/WT}$ mice (n=9 neurons, 3 mice) had higher BK current density compared to *Kcnma1*$^{WT/WT}$ at −30 mV only (†p=0.0321). (**C**) BK current density was not different in *Kcnma1*$^{H444Q/WT}$ neurons (n=7 neurons, 2 mice) compared to *Kcnma1*$^{WT/WT}$ (n=6 neurons, 3 mice).

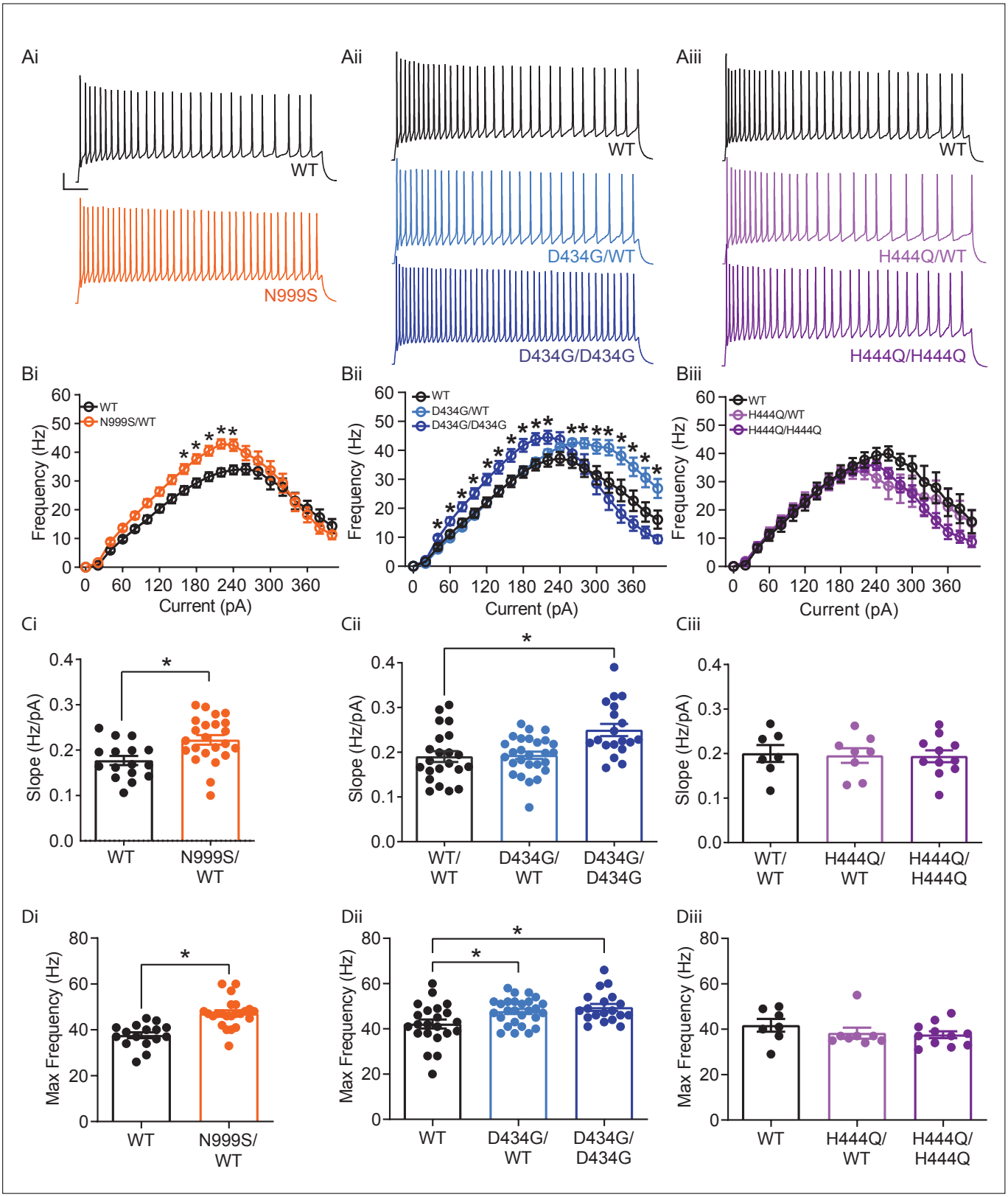

Figure 3. Increased intrinsic excitability in *Kcnma1*$^{N999S/WT}$, *Kcnma1*$^{D434G/WT}$, and *Kcnma1*$^{D434G/D434G}$ granule neurons. In current-clamp mode, step currents from 0 to 400 pA were applied to dentate granule neurons under the same ionic conditions used to record BK currents. (Ai–Aiii) Representative AP trains elicited from the 200 pA current injection step in WT and transgenic neurons. Scale bar: 20 mV, 100 ms. (Bi–Biii) Input-output relationship for firing frequency versus step current injection. Data are presented as mean ± SEM. *p<0.05, two-way repeated measures ANOVA with Bonferroni post

Figure 3 continued on next page

Figure 3 continued

hoc. (Bi) *Kcnma1*$^{N999S/WT}$ (n=23 neurons, 5 mice) firing was higher than *Kcnma1*$^{WT/WT}$ (n=16 neurons, 5 mice) at 160 pA (p=0.0426), 180 pA (p=0.0143), 200 (p=0.0068), 220 pA (p=0.0009), and 240 pA (p=0.0337) current steps. (Bii) *Kcnma1*$^{D434G/WT}$ (n=27 neurons, 5 mice) firing was higher than *Kcnma1*$^{WT/WT}$ (n=22 neurons, 5 mice) at 260 pA (p=0.0452), 280 (p=0.0314), 300 (p=0.0351), 320 (p=0.0177), 340 (p=0.0309), 360 (p=0.0358), 380 (p=0.0312), and 400 (p=0.0444) current steps. *Kcnma1*$^{D434G/D434G}$ (n=19 neurons, 4 mice) firing was higher than *Kcnma1*$^{WT/WT}$ at 40 pA (p=0.0266), 60 (p=0.0233), 80 (p=0.0277), 100 (p=0.0130), 120 (p=0.0074), 140 (p=0.0119), 160 (p=0.0084), 180 (p=0.0063), 200 (p=0.0059), and 220 (p=0.0261) current steps. (Biii) *Kcnma1*$^{H444Q/WT}$ (n=8 neurons, 2 mice) and *Kcnma1*$^{H444Q/H444Q}$ (n=11 neurons, 2 mice) firing was not different than *Kcnma1*$^{WT/WT}$ (n=7 neurons, 1 mouse) at any current step (p=0.3222). (Ci–Ciii) Initial slope for the firing rate gain between 0 and 160 pA current injections. Data are presented as mean ± SEM, with individual data points. (Ci) *Kcnma1*$^{N999S/WT}$ firing slope was increased compared to WT (*p=0.0034; t-test). (Cii) *Kcnma1* $^{D434G/D434G}$ firing slope was increased compared to WT (*p=0.0051; one-way ANOVA), *Kcnma1* $^{D434G/WT}$ slopes were unchanged (p=0.9774). (Ciii) *Kcnma1*$^{H444Q/WT}$ and/or *Kcnma1*$^{H444Q/H444Q}$ firing slopes were not different than WT (p=0.9658). (Di–Diii) Maximum firing frequency. Data are presented as mean ± SEM. (Di) Maximal firing from *Kcnma1*$^{N999S/WT}$ neurons was increased compared to WT (*p<0.0001; t-test). (Dii) Maximal firing from *Kcnma1* $^{D434G/WT}$ and *Kcnma1* $^{D434G/D434G}$ neurons was increased compared to WT (*p=0.0387 and p=0.0111, respectively; one-way ANOVA). (Diii) Maximal firing from *Kcnma1*$^{H444Q/WT}$ and/or *Kcnma1*$^{H444Q/H444Q}$ neurons was not different than WT (p=0.4625; one-way ANOVA). Passive membrane properties for this dataset appear in ***Figure 3—figure supplement 1***. Action potential waveform analysis for this dataset appears in ***Figure 3—figure supplement 2***.

Figure 3-figure supplement 1

	N	Resting membrane potential (mV)	Input resistance (MΩ)	Membrane time constant (ms)	Membrane capacitance (pF)
Kcnma1$^{WT/WT}$	16	-80 ± 1	324 ± 12	24 ± 1	76 ± 2
Kcnma1$^{N999S/WT}$	23	-80 ± 1	351 ± 13	25 ± 1	72 ± 2
Kcnma1$^{WT/WT}$	22	-82 ± 1	364 ± 15	27 ± 1	75 ± 2
Kcnma1$^{D434G/WT}$	27	-83 ± 1	344 ± 11	30 ± 1	86 ± 2*
Kcnma1$^{D434G/D434G}$	19	-82 ± 1	371 ± 14	27 ± 1	74 ± 3
Kcnma1$^{WT/WT}$	7	-80 ± 2	320 ± 18	22 ± 2	68 ± 3
Kcnma1$^{H444Q/WT}$	8	-82 ± 1	342 ± 35	22 ± 2	67 ± 5
Kcnma1$^{H444Q/H444Q}$	11	-79 ± 1	345 ± 16	22 ± 1	65 ± 3

Figure 3—figure supplement 1. Passive membrane properties. Data are presented as mean ± SEM. Resting membrane potential (RMP) was −80 to −82 mV across WT controls. No significant depolarizations were observed between littermate controls and *Kcnma1*$^{N999S/WT}$, *Kcnma1*$^{D434G/D434G}$, *Kcnma1*$^{H444Q/WT}$, and *Kcnma1*$^{H444Q/H444Q}$ dentate granule neurons (p>0.05, unpaired t-test and one-way ANOVA, respectively). Similarly, the range for input resistance (R_i) was 320–364 MΩ for WT neurons and was not different in any transgenic condition. These results are consistent with previous studies in dentate granule cells finding no effect of BK channel inhibition on RMP or R_i (***Bock and Stuart, 2016***; ***Brenner et al., 2005***). The only condition showing a difference from the respective WT control was a greater membrane capacitance (C_m) in *Kcnma1*$^{D434G/WT}$ neurons (*p=0.0036). An explanation for this change in C_m is unclear from the data. However, this difference could have the potential to reduce the firing gain at lower current injections, preventing the *Kcnma1*$^{D434G/WT}$ input-output curve from looking similar to *Kcnma1*$^{N999S/WT}$ (***Figure 3Bi, Bii***).

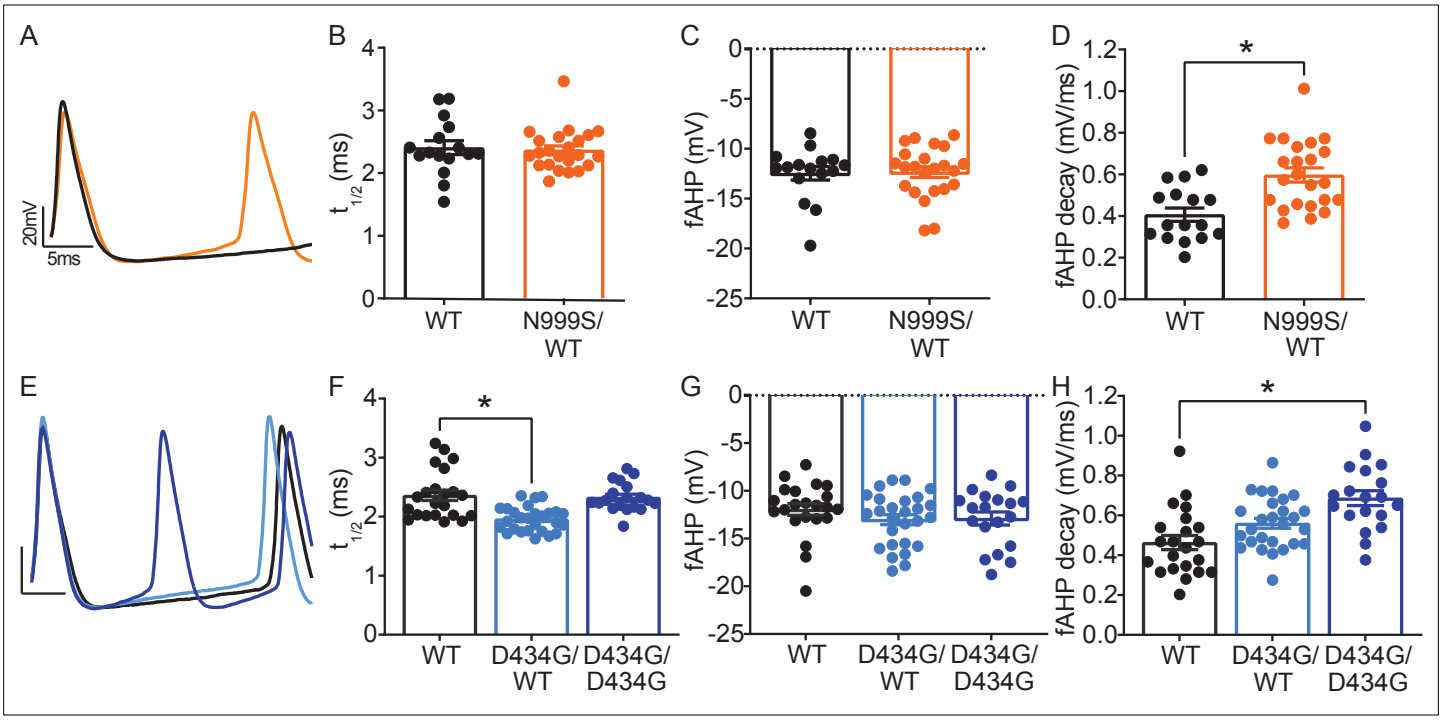

Figure 3—figure supplement 2. *Kcnma1*$^{N999S/WT}$, *Kcnma1*$^{D434G/WT}$, and *Kcnma1*$^{D434G/D434G}$ action potential waveforms. (**A**) Superimposed *Kcnma1*$^{N999S/WT}$ and *Kcnma1*$^{WT/WT}$ waveforms from the 10th action potential at the 200 pA current injection from data in ***Figure 3***. (**B**) Action potential half-width ($t_{1/2}$) was not different in *Kcnma1*$^{N999S/WT}$ neurons versus WT controls (p=0.6617; Mann-Whitney test). (**C**) Fast afterhyperpolarizations (fAHP) amplitude was not different in *Kcnma1*$^{N999S/WT}$ neurons versus WT controls (p=9214; Mann-Whitney test). (**D**) AHP decay 3 ms after the peak was faster in *Kcnma1*$^{N999S/WT}$ neurons (*Kcnma1*$^{N999S/WT}$ 0.60±0.03 mV/ms) compared to WT controls (0.41±0.03 mV/ms, *p=0.0002; t-test). In panels B-D, *Kcnma1*$^{N999S/WT}$ (n = 23 neurons) and *Kcnma1*$^{WT/WT}$ (n = 16 neurons). (**E**) Superimposed *Kcnma1*$^{D434G/D434G}$, *Kcnma1*$^{D434G/WT}$, and *Kcnma1*$^{WT/WT}$ waveforms from the 10th action potential at the 200 pA current injection from data in ***Figure 3***. (**F**) $t_{1/2}$ was different in *Kcnma1*$^{D434G/WT}$ (*p=0.0002; Kruskal-Wallis test), but not *Kcnma1*$^{D434G/D434G}$ neurons (p=0 > 0.9999). (**G**) fAHP amplitudes were comparable in *Kcnma1*^{D434G} mice (p=0.3441; Kruskal-Wallis test). (**H**) AHP decay 3 ms after the peak was faster in *Kcnma1*$^{D434G/D434G}$ neurons (0.69±0.04 mV/ms) compared to WT controls (0.46±0.04 mV/ms, *p=0.0002), but not in *Kcnma1*$^{D434G/WT}$ (0.56±0.02 mV/ms, p=0.0620; one-way ANOVA). In panels F-H, *Kcnma1*$^{D434G/D434G}$ (n = 19 neurons), *Kcnma1*$^{D434G/WT}$ (n = 27 neurons), and *Kcnma1*$^{WT/WT}$ (n = 22 neurons). Data are presented as mean ± SEM, with individual data points.

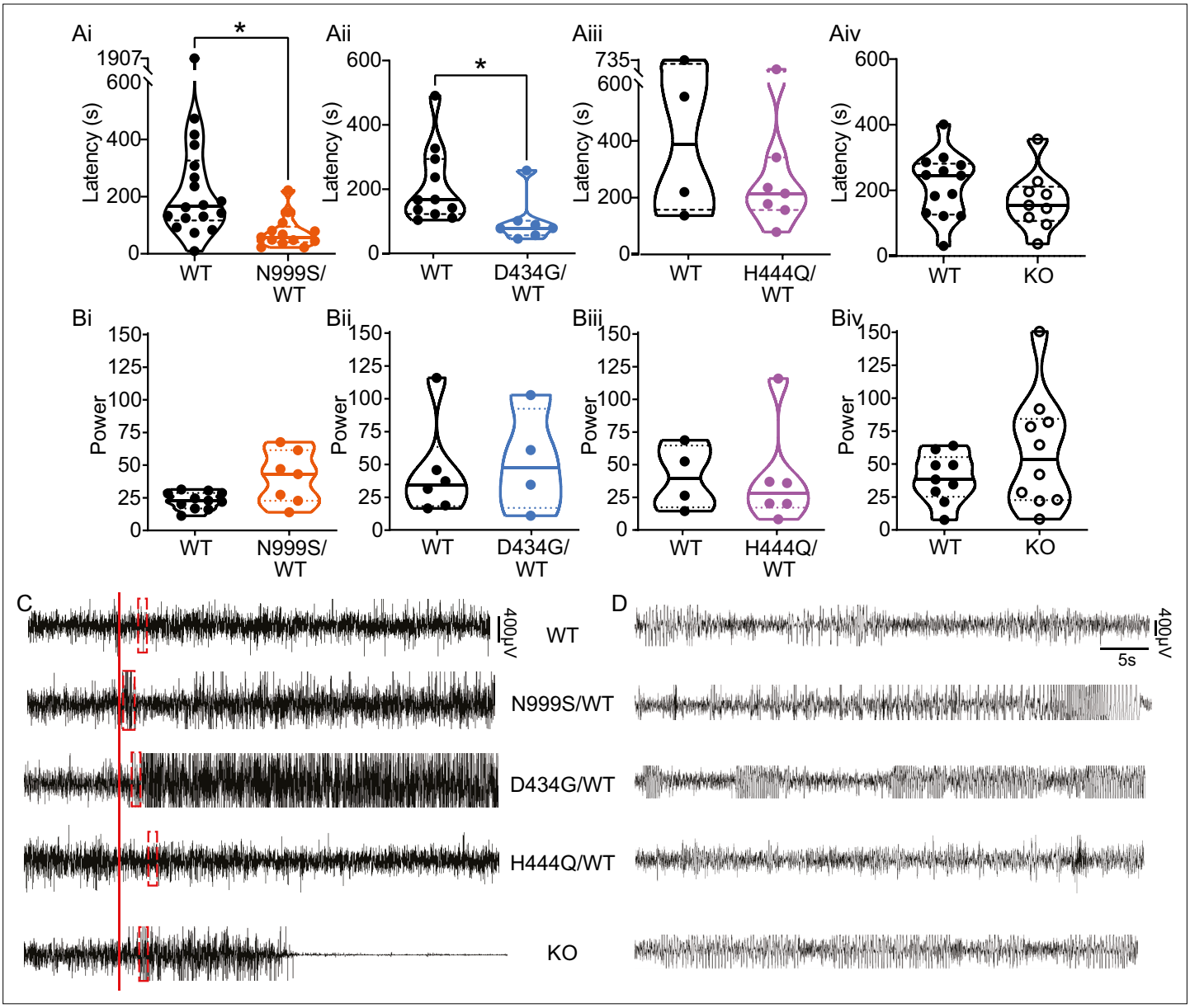

Figure 4. Pentylenetetrazol (PTZ)-induced seizures in mice. (Ai–Aiv) Latency to initial seizure after PTZ injection. Data are individual mice with median and inter-quartile range. (Ai) Latency was decreased in *Kcnma1*$^{N999S/WT}$ mice (n=13) compared to *Kcnma1*$^{WT/WT}$ (n=18, *p=0.0006; Mann-Whitney test). (Aii) Latency was decreased in *Kcnma1*$^{D434G/WT}$ mice (n=7) compared to *Kcnma1*$^{WT/WT}$ (n=11, *p=0.0041; Mann-Whitney test). (Aiii) Seizure latency was comparable between *Kcnma1*$^{H444Q/WT}$ (n=7) and *Kcnma1*$^{WT/WT}$ (n=4, p=0.5273; Mann-Whitney test). (Aiv) No differences were found in seizure latency between *Kcnma1*$^{-/-}$ (n=9) and *Kcnma1*$^{+/+}$ mice (n=13, p=0.2282; Mann-Whitney test). (Bi–iv) Total EEG power after PTZ injection (y-axis in $\mu V^2/Hz \times 10^2$). Data are individual mice with median and inter-quartile range. (Bi) EEG power was not different between *Kcnma1*$^{N999S/WT}$ (n=7) and *Kcnma1*$^{WT/WT}$ (n=11, p=0.0619; t-test). (Bii) *Kcnma1*$^{D434G/WT}$ (n=4) was not different from *Kcnma1*$^{WT/WT}$ (n=6, p=0.7563; t-test). (Biii) *Kcnma1*$^{H444Q/WT}$ (n=6) was not different from *Kcnma1*$^{WT/WT}$ (n=4, p=0.9641; t-test). (Biv) *Kcnma1*$^{-/-}$ (n=10) was not different from *Kcnma1*$^{+/+}$ (n=9, p=0.2134; t-test). (**C**) Representative EEG traces over 45 min at baseline and after PTZ injection (red line). (**D**) Expanded EEG traces for the first seizure indicated with the red boxes in (**C**). Representative videos for this dataset appear in ***Figure 4—videos 1–4***.

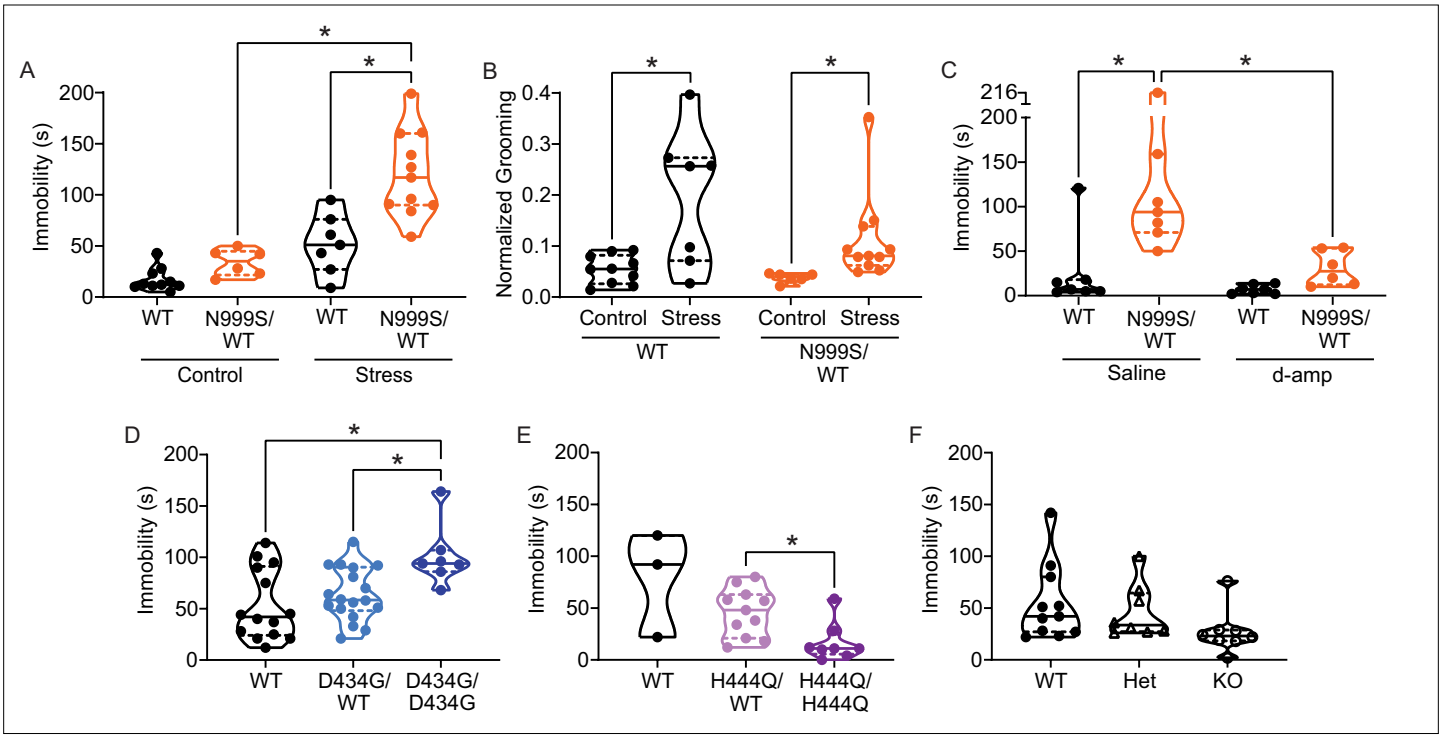

Figure 5. Stress-induced paroxysmal dyskinesia. (**A**) Control: Without restraint stress, there was no difference in the time spent immobile between *Kcnma1*$^{WT/WT}$ (n=10) and *Kcnma1*$^{N999S/WT}$ mice (n=6, p>0.9999; two-way ANOVA with Bonferroni post hoc). Restraint stress: Immobility time was longer for restrained *Kcnma1*$^{N999S/WT}$ mice (n=11) compared to *Kcnma1*$^{WT/WT}$ (n=7, *p=0.0001; one-way ANOVA), and between restrained *Kcnma1*$^{N999S/WT}$ mice (n=11) compared to unrestrained *Kcnma1*$^{N999S/WT}$ mice (n=6, *p<0.0001). In contrast, unrestrained *Kcnma1*$^{WT/WT}$ mice (n=10) had no differences from restrained *Kcnma1*$^{WT/WT}$ mice (n=7, p=0.1174). (**B**) Grooming behavior increased in restrained *Kcnma1*$^{WT/WT}$ mice (n=7) compared to unrestrained *Kcnma1*$^{WT/WT}$ mice (n=10, *p=0.0300; t-test), and in restrained *Kcnma1*$^{N999S/WT}$ mice (n=11) compared to unrestrained *Kcnma1*$^{N999S/WT}$ mice (n=6, *p=0.0174; t-test). (**C**) Immobility time was longer for saline-treated *Kcnma1*$^{N999S/WT}$ mice (n=7) compared to *Kcnma1*$^{WT/WT}$ (n=7, *p=0.0018) and d-amp-treated *Kcnma1*$^{N999S/WT}$ mice (n=6, *p=0.0053; two-way ANOVA with Bonferroni post hocs). There was no difference between d-amp-treated *Kcnma1*$^{WT/WT}$ mice (n=7), d-amp-treated *Kcnma1*$^{N999S/WT}$ mice (n=6, p>0.9999), and saline-treated *Kcnma1*$^{WT/WT}$ mice (n=7, p>0.9999). (**D**) After restraint, *Kcnma1*$^{D434G/D434G}$ mice (n=7) spent more time immobile compared to *Kcnma1*$^{WT/WT}$ mice (n=14, *p=0.0166; one-way ANOVA). However, *Kcnma1*$^{D434G/WT}$ mice were not different (n=18, p=0.7174). (**E**) Immobility time was shorter in restrained *Kcnma1*$^{H444Q/H444Q}$ mice (n=8) compared to *Kcnma1*$^{H444Q/WT}$ mice (n=11, *p=0.0081; t-test). *Kcnma1*$^{WT/WT}$ mice were not included in the statistical analysis due to small sample size (n=3). (**F**) *Kcnma1*$^{-/-}$ mice (n=8) had reduced immobility compared to *Kcnma1*$^{-/+}$ mice (n=8) and *Kcnma1*$^{+/+}$ mice (n=11, p=0.0535; Kruskal-Wallis test). Data are individual mice with median and inter-quartile range. Representative videos for this dataset appear in ***Figure 5—video 5–1***.

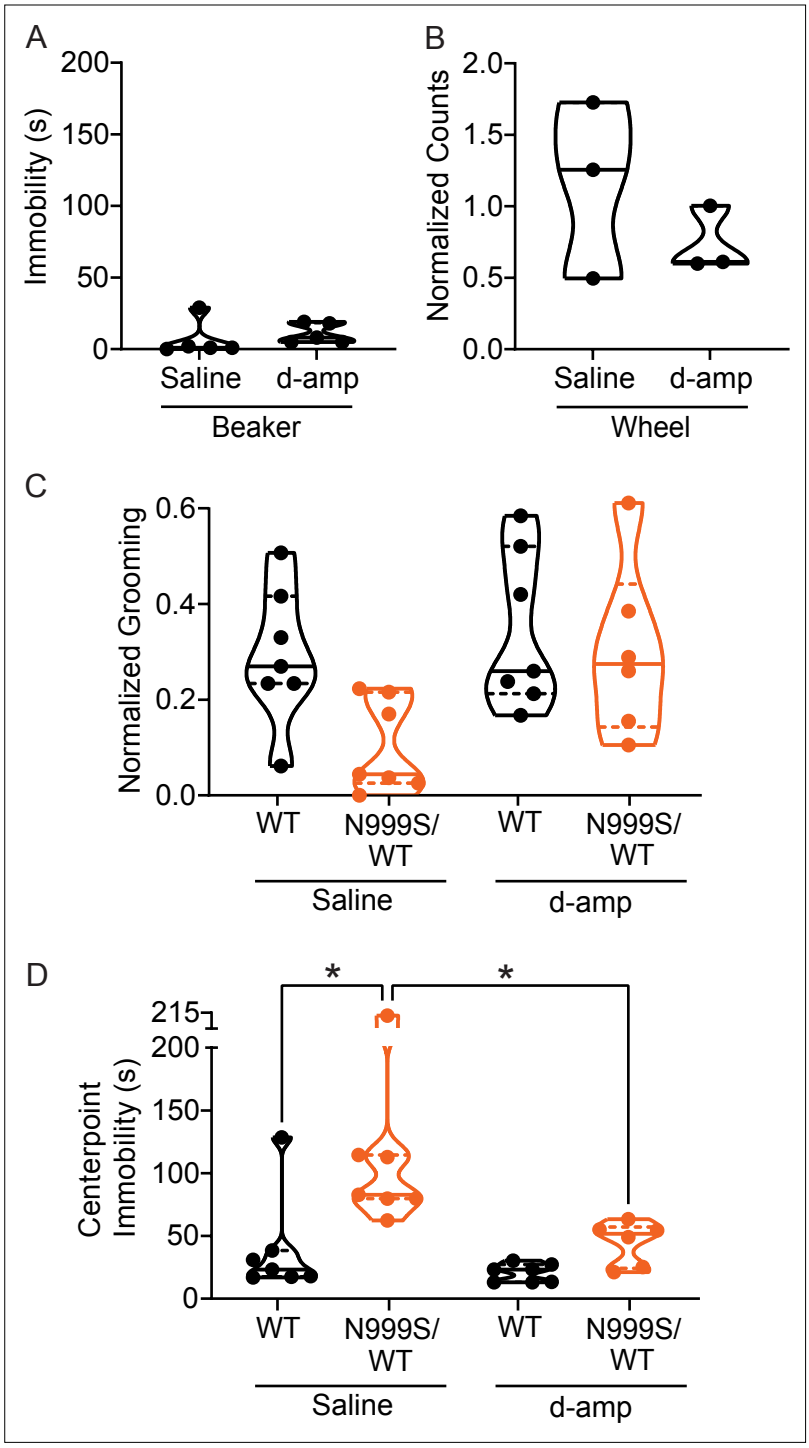

Figure 5—figure supplement 1. Locomotor, stress, and immobility analysis methodology controls in *Kcnma1*$^{N999S/WT}$ mice. (**A**) Unrestrained WT C57BL6J-background mice were used to test for any baseline effects of the injection procedures (saline) or d-amp (0.5 mg/kg) on immobility in the beaker assay, assessed 30 min after injection. No difference between saline (n=5) and d-amp-injected mice (n=5, p=0.1429, Mann-Whitney test) was observed. (**B**) Unrestrained WT C57BL6J-background mice were used to test for any baseline effects of d-amp (0.5 mg/kg) on locomotor wheel running activity. Normalized activity after injection was comparable between saline (n=3) and d-amp-injected mice (n=3, p=0.7000, Mann-Whitney test). (**C**) *Kcnma1*$^{WT/WT}$ and *Kcnma1*$^{N999S/WT}$ mice used in the restraint-induced immobility assay in main ***Figure 5C*** were scored for grooming behavior after d-amp treatment. No significant differences were present between saline-injected *Kcnma1*$^{WT/WT}$ mice (n=7), saline-injected *Kcnma1*$^{N999S/WT}$ mice (n=7, p=0.1456), and d-amp-injected *Kcnma1*$^{WT/WT}$ mice (n=7, p>0.9999, two-way ANOVA

Figure 5—figure supplement 1 continued on next page

Figure 5—figure supplement 1 continued

with Bonferroni post hoc). Additionally, d-amp-injected *Kcnma1*$^{N999S/WT}$ mice (n=6) were not different from d-amp-injected *Kcnma1*$^{WT/WT}$ mice (n=7, p>0.9999) and saline-injected *Kcnma1*$^{N999S/WT}$ mice (n=7, p=0.1461). (**D**) Center point movement parameters were calculated using automated analysis (EthoVision software) from the same videos of restraint stress-induced immobility in main ***Figure 5C***. Immobility time was longer for saline-injected *Kcnma1*$^{N999S/WT}$ mice (n=7) compared to *Kcnma1*$^{WT/WT}$ (n=7, *p=0.0077) and d-amp-injected *Kcnma1*$^{N999S/WT}$ mice (n=6, *p=0.0223; two-way ANOVA with Bonferroni post hoc). In contrast, d-amp-injected *Kcnma1*$^{N999S/WT}$ mice (n=6) were not different from d-amp-injected *Kcnma1*$^{WT/WT}$ mice (n=7, p>0.9999) or saline-injected *Kcnma1*$^{WT/WT}$ mice (n=7, p>0.9999). All data are median and inter-quartile range.

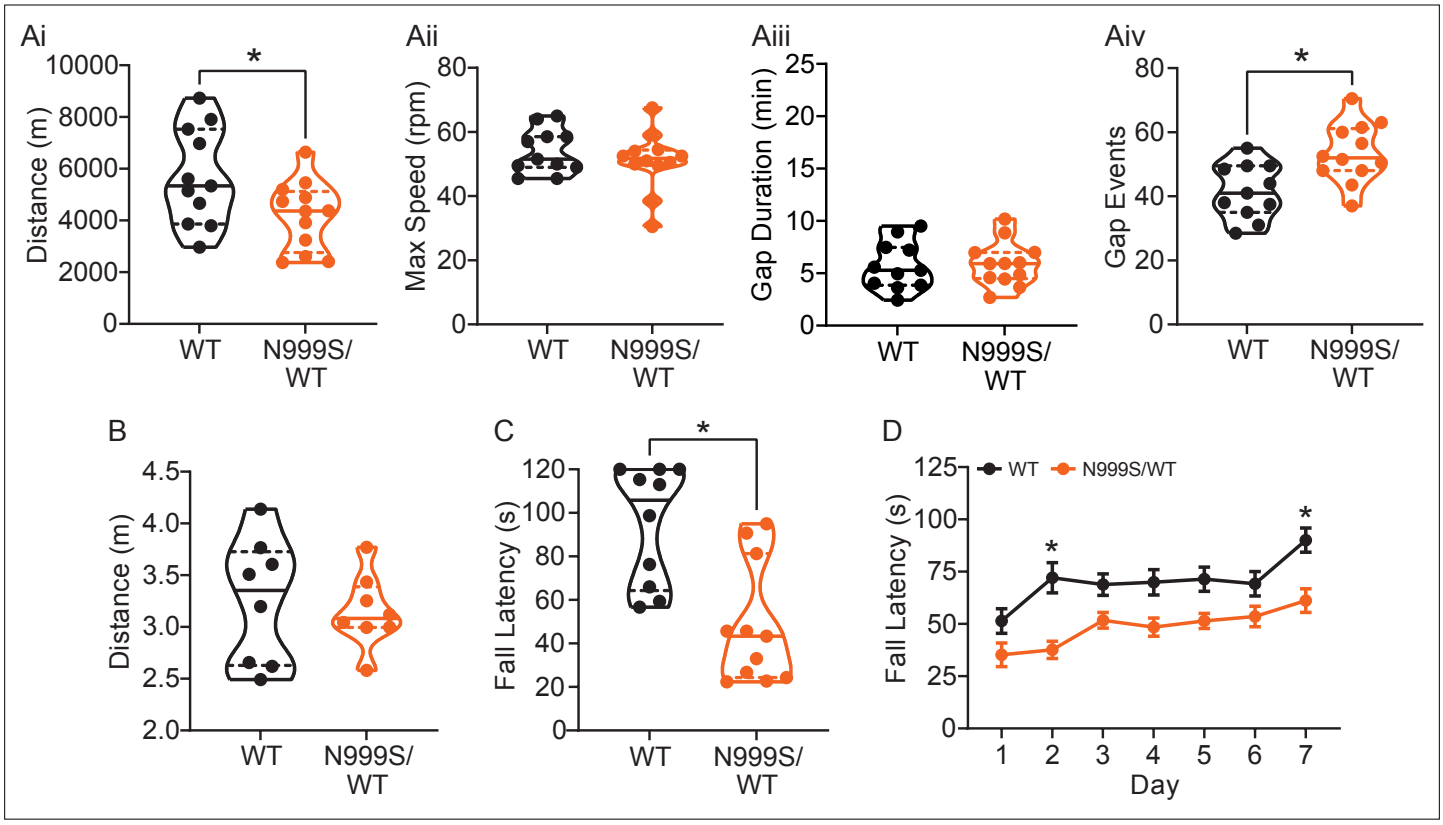

Figure 6. Motor coordination in *Kcnma1*$^{N999S/WT}$ mice. (**A**) Locomotor wheel running parameters calculated from average activity counts over 48 hr from singly housed mice with free access to wheels. (Ai) Distance covered was reduced for *Kcnma1*$^{N999S/WT}$ (n=12) compared to *Kcnma1*$^{WT/WT}$ mice (n=11, *p=0.0411; t-test). (Aii) Maximum speed was comparable between *Kcnma1*$^{N999S/WT}$ (n=11) and *Kcnma1*$^{WT/WT}$ mice (n=12, p=0.3618; t-test). (Aiii) Duration of time off wheels (gap duration) was comparable between *Kcnma1*$^{N999S/WT}$ (n=11) and *Kcnma1*$^{WT/WT}$ mice (n=12, p=0.8281; t-test). (Aiv) Number of times the mouse was off the wheel (gap events) was higher for *Kcnma1*$^{N999S/WT}$ (n=12) compared to *Kcnma1*$^{WT/WT}$ mice (n=11, *p=0.0040; t-test). (**B**) Open field assay. *Kcnma1*$^{N999S/WT}$ mice (n=8) covered the same distance as *Kcnma1*$^{WT/WT}$ mice (n=8) in a 15 min trial (p=0.6973; t-test). (**C**) Acute muscle strength was tested by hanging mice from a stationary platform (cage lid) for 120 s. Fall latency was lower in *Kcnma1*$^{N999S/WT}$ (n=11) compared to *Kcnma1*$^{WT/WT}$ mice (n=10, *p=0.0014; Mann-Whitney test) indicating weaker grip strength. (**D**) Rotarod assay. Fall latency was lower for *Kcnma1*$^{N999S/WT}$ mice (n=11) on day 2 (*p=0.0045) and day 7 (*p=0.0124) compared to *Kcnma1*$^{N999S/WT}$ mice (n=12). Motor learning was observable as an improvement in fall latency times across the three trials on each day (data not shown), suggesting the overall impairment was related to motor coordination and not learning. Data are presented as individual data points with median and inter-quartile range (**A–C**) and mean ± SEM (**D**). Results for these assays with *Kcnma1*^{D434G}, *Kcnma1*^{H444Q}, and *Kcnma1*$^{-/-}$ mice appear in ***Figure 6—figure supplements 1 and 2***. For these assays, the baseline motor coordination severity fell in the series *Kcnma1*$^{-/-}$>*Kcnma1*$^{D434G/D434G}$ > *Kcnma1*$^{N999S/WT}$>*Kcnma1*$^{H444Q/H444Q}$.

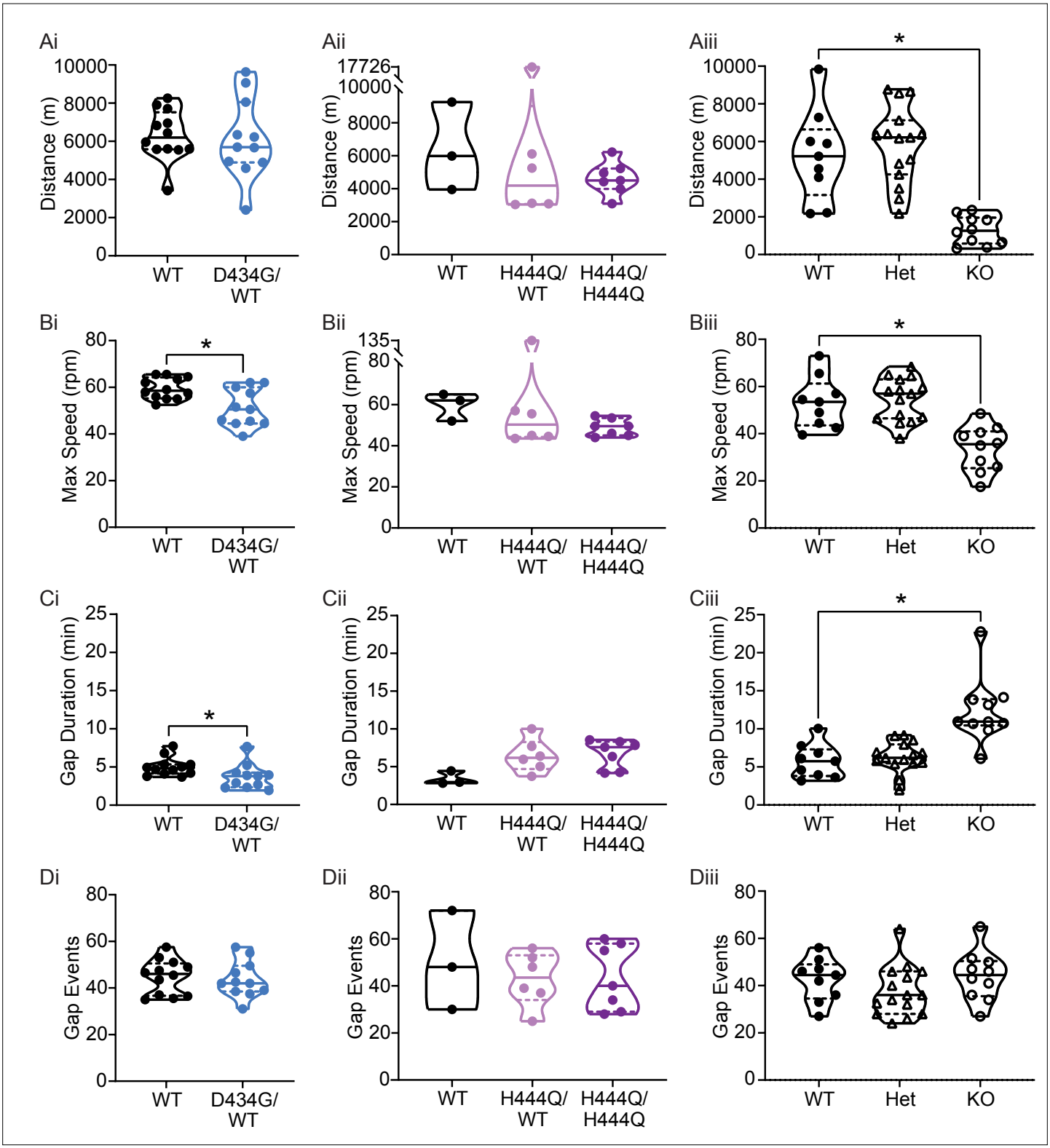

Figure 6—figure supplement 1. Motor coordination in *Kcnma1*^{D434G}, *Kcnma1*^{H444Q}, and *Kcnma1*$^{-/-}$ mice. (Ai) Distance was comparable between *Kcnma1*$^{D434G/WT}$ (n=11) and *Kcnma1*$^{WT/WT}$ mice (n=12, p=0.8118; t-test). (Aii) Distance was comparable between *Kcnma1*$^{H444Q/H444Q}$ (n=7) and *Kcnma1*$^{H444Q/WT}$ (n=6, p=0.4880; t-test). *Kcnma1*$^{WT/WT}$ mice were not included in statistical analysis in panels Aii–Dii due to small sample size. (Aiii) Distance was reduced for *Kcnma1*$^{-/-}$ (n=10) compared *Kcnma1*$^{+/+}$ (n=9, *p=0.0032), but not for *Kcnma1*$^{-/+}$ mice (n=15, p=0.9057; one-way ANOVA). (Bi) Maximum speed was lower for *Kcnma1*$^{D434G/WT}$ (n=11) compared to *Kcnma1*$^{WT/WT}$ mice (n=12, *p=0.0085; t-test). (Bii) Maximum speed was comparable between *Kcnma1*$^{H444Q/}$

Figure 6—figure supplement 1 continued on next page

Figure 6—figure supplement 1 continued

^{H444Q} (n=7) and *Kcnma1*$^{H444Q/WT}$ (n=6, p=0.3634; t-test). (Biii) Maximum speed was lower for *Kcnma1*$^{-/-}$ (n=10) compared to *Kcnma1*$^{+/+}$ (n=9, *p=0.0024), but not for *Kcnma1*$^{-/+}$ mice (n=15, p=0.9871; one-way ANOVA). (Ci) Gap duration was reduced for *Kcnma1*$^{D434G/WT}$ (n=11) compared to *Kcnma1*$^{WT/WT}$ mice (n=12, *p=0.0467; t-test). (Cii) Gap duration was comparable between *Kcnma1*$^{H444Q/H444Q}$ (n=7) and *Kcnma1*$^{H444Q/WT}$ mice (n=6, p=0.8326; t-test). (Ciii) Gap duration was higher in *Kcnma1*$^{-/-}$ (n=10) compared to *Kcnma1*$^{+/+}$ mice (n=9, *p=0.0026), but not for *Kcnma1*$^{-/+}$ mice (n=15, p=0.8987; one-way ANOVA). (Di) Gap events were comparable between *Kcnma1*$^{D434G/WT}$ (n=11) and *Kcnma1*$^{WT/WT}$ mice (n=12, p=0.7425; t-test). (Dii) Gap events were comparable between *Kcnma1*$^{H444Q/H444Q}$ (n=7) and *Kcnma1*$^{H444Q/WT}$ (n=6, p=0.9341; t-test). (Diii) Gap events were comparable for *Kcnma1*$^{-/-}$ (n=10), *Kcnma1*$^{-/+}$ (n=15), and *Kcnma1*$^{+/+}$ mice (n=9, p=0.3047; one-way ANOVA). All data are presented as individual data points with median and inter-quartile range.

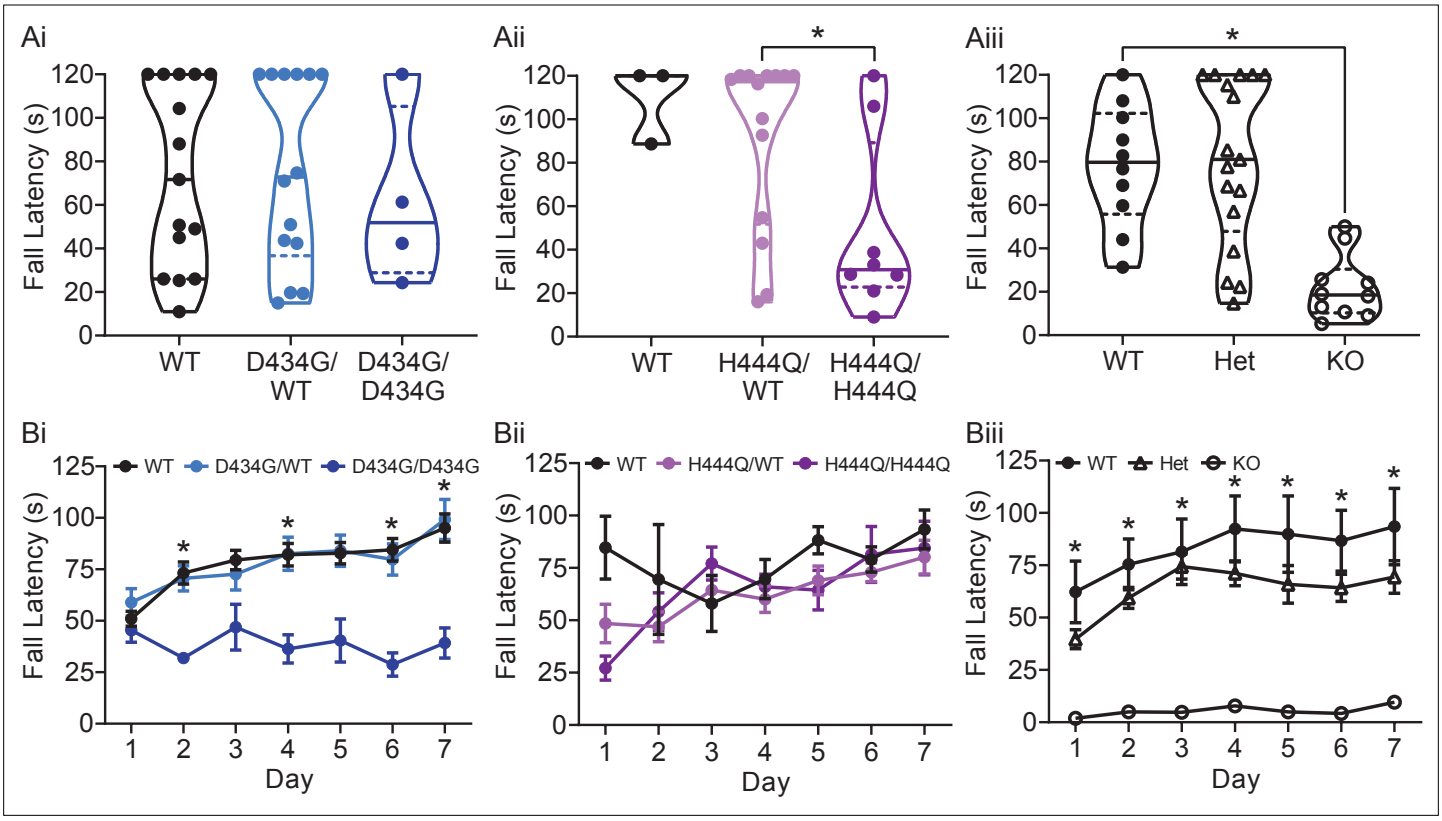

Figure 6—figure supplement 2. Hanging wire and rotarod in *Kcnma1*^{D434G}, *Kcnma1*^{H444Q}, and *Kcnma1*$^{-/-}$ mice. (**A**i-iii) Hanging wire assay. Data are presented as individual data points with median and inter-quartile range. (**Ai**) Fall latency was comparable for *Kcnma1*$^{D434G/D434G}$ (n=4), *Kcnma1*$^{D434G/WT}$ (n=11), and *Kcnma1*$^{WT/WT}$ mice (n=11, p=0.8329; Kruskal-Wallis test), providing no evidence for acute differences in strength. (**Aii**) Fall latency was reduced for *Kcnma1*$^{H444Q/H444Q}$ (n=8) compared to *Kcnma1*$^{H444Q/WT}$ mice (n=14, *p=0.0465; Mann-Whitney test). *Kcnma1*$^{WT/WT}$ mice were not included in the statistical analysis due to small sample size (n=3). (Aiii) Fall latency times were lower for *Kcnma1*$^{-/-}$ mice (n=10) compared to *Kcnma1*$^{+/+}$ mice (n=10, *p=0.0036), but not for *Kcnma1*$^{-/+}$ mice (n=17, p>0.9999; Kruskal-Wallis test). No *Kcnma1*$^{-/-}$ mouse had the ability to hang on longer than 60 s, consistent with previous reports (***Meredith et al., 2004***; ***Sausbier et al., 2004***; ***Wang et al., 2020***; ***Yao et al., 2021***). (Bi-iii) Time to fall in rotarod assay. Data are presented as mean ± SEM. (Bi) Fall latency was lower for *Kcnma1*$^{D434G/D434G}$ mice (n=4) on day 2 (p<0.0001), day 4 (p=0.0030), day 6 (p<0.0001), and day 7 (p=0.0009) compared to *Kcnma1*$^{WT/WT}$ mice (n=21), but were comparable in *Kcnma1*$^{D434G/WT}$ mice (n=18; *p<0.05, repeated measures ANOVA with Bonferroni post hoc). (Bii) Fall latency was not different between *Kcnma1*$^{H444Q/H444Q}$ (n=7) and *Kcnma1*$^{H444Q/WT}$ (n=10; repeated measures ANOVA with Bonferroni post hoc); however, performance was highly variable, reducing the ability to make a firm conclusion from this data. *Kcnma1*$^{WT/WT}$ mice were not included in the statistical analysis due to small sample size (n=2). (Biii) Fall latency was lower for *Kcnma1*$^{-/-}$ mice (n=6) on day 1 (p=0.0277), day 2 (p=0.0056), day 3 (p=0.0122), day 4 (p=0.0081), day 5 (p=0.0166), day 6 (p=0.0071), and day 7 (p=0.0168) compared to *Kcnma1*$^{+/+}$ mice (n=6), but were comparable in *Kcnma1*$^{-/+}$ mice (n=13; *p<0.05, repeated measures ANOVA with Bonferroni post hoc).